Heliyon 10 (2024) e32183

Contents lists available at ScienceDirect

Heliyon

journal homepage: www.cell.com/heliyon

Research article

Thermal-responsive β-cyclodextrin-based magnetic hydrogel as a *de novo* nanomedicine for chemo/hyperthermia treatment of cancerous cells

Morteza Eskandani [a], Rana Jahanban-Esfahlan [b], Mohammad Mehdi Sadughi [c], Mehdi Jaymand [d,e,*]

[a] *Research Center for Pharmaceutical Nanotechnology, Biomedicine Institute, Tabriz University of Medical Sciences, Tabriz, Iran*
[b] *Department of Medical Biotechnology, School of Advanced Medical Sciences, Tabriz University of Medical Sciences, Tabriz, Iran*
[c] *Islamic Azad University, Central Tehran Branch, Tehran, Iran*
[d] *Nano Drug Delivery Research Center, Health Technology Institute, Kermanshah University of Medical Sciences, Kermanshah, Iran*
[e] *Students Research Committee, Kermanshah University of Medical Sciences, Kermanshah, Iran*

A R T I C L E I N F O

Keywords:
β-Cyclodextrin
Poly(*N*-isopropylacrylamide)
Magnetic hydrogel
Thermal-responsive
Chemo/hyperthermia therapy
Cancer

A B S T R A C T

A novel thermal-responsive β-cyclodextrin-based magnetic hydrogel [β-cyclodextrin-*graft*-poly(*N*-isopropylacrylamide)/Fe_3O_4 (β-CD-*g*-PNIPAAm/Fe_3O_4)] was fabricated as a novel nanomedicine for chemo/hyperthermia treatment of cancer cells. Firstly, β-CD was modified by maleic anhydride (MA) followed by copolymerization with NIPAAm monomer and thiol-end capped Fe_3O_4 nanoparticles (NPs) in the presence of a crosslinker through acrylamide–thiol polymerization system to afford a magnetic hydrogel. The saturation magnetization (δ_s) value for developed hydrogel was determined to be 8.2 emu g^{-1}. The hydrogel was physically loaded with an anticancer agent, doxorubicin hydrochloride (Dox). The encapsulation efficiency (EE) of drug into the hydrogel was obtained as 73 %. The system represented acceptable thermal-triggered drug release behavior that best fitted with Higuchi model, demonstrating the release of drug is mostly controlled by diffusion mechanism. The anticancer performance of the β-CD-*g*-PNIPAAm/Fe_3O_4-Dox was evaluated using MCF7 cells by MTT-assay. In addition, flow cytometry analyses showed considerable cellular uptake of Dox in the cells treated with β-CD-*g*-PNIPAAm/Fe_3O_4-Dox (~70 %) compared to free Dox (~28 %). As results, in time period of 48 h by combination of chemo- and hyperthermia-therapies, the developed system displayed greater anticancer efficiency than the free Dox.

1. Introduction

Canncer is the secound principal cause of death after cariovascular deasies as the World Health Organization (WHO) statistic's. Despite some progresses in the cancer treatment approaches, thematic side effects, including gastrointestinal problems, neurological effects, and fatigue are still challenging [1–6]. The most extensively cancer treatment methods are chemotherapy, radiotherapy, surgery, hormonal therapy, and immunotherapy. In addition, some newly developed approaches, such as hyperthermia therapy,

* Corresponding author. Nano Drug Delivery Research Center, Health Technology Institute, Kermanshah University of Medical Sciences, Kermanshah, Iran.
E-mail addresses: m_jaymand@yahoo.com, m.jaymand@gmail.com, mehdi.jaymand@kums.ac.ir (M. Jaymand).

https://doi.org/10.1016/j.heliyon.2024.e32183
Received 26 October 2023; Received in revised form 26 May 2024; Accepted 29 May 2024
Available online 30 May 2024

photodynamic therapy, and photothermal therapy can be employed as efficient cancer treatment methods [7–10]. The engineering of nanostructures for biomedical applications, define as nanomedicine, has opening new opportunities toward the advanced drug delivery systems (DDSs) in chemotherapy of cancer [11–14]. In this regard, DDSs based on hydrogels have attracted great attention because of their fascinating physicochemical (*e.g.,* proper stability in various pHs, soft texture, high porosity, and excellent hydrophilicity) and biological (*e.g.,* comparable structure to native extracellular matrix (ECM), excellent biocompatibility and biodegradability in most cases, and non-toxic biodegradation by-products) features [15–18]. More interestingly, incorporation of natural macromolecules (*e.g.,* polysaccharides) into a hydrogel can improve the biological functions of hydrogels [19]. β-Cyclodextrin (β-CD) is a well-known cyclic oligosaccharide (formed from seven glucose units) with amphiphilic nature. Owing to inherent physicochemical/biological properties, β-CD is widely applied in the fabrication of DDSs. The amphiphilic nature of this oligosaccharide provide possibility for the loading of both hydrophilic and hydrophobic pharmaceuticals that allow combination chemotherapy [20–22].

On the other hand, stimuli-responsive DDSs allows the "*smart*" release of loaded cargo at the cancerous tissues mainly due to abnormal physicochemical micro-environment of cancerous cells (known as internal stimuli) or by applying external triggers [23–28]. Among the various stimuli, thermal stimuli attracted significant interest due to its simplicity as well as the higher temperature of tumorous tissues than the healthy tissues. Poly(*N*-isopropylacrylamide) (PNIPAAm) is the mostly recognized thermal-sensitive polymer that displayed a critical solution temperature (LCST) at around 32 °C [29]. The LCST of PNIPAAm could be engineered nearby the body temperature (37 °C) and more especially around 40 °C *via* the copolymerization with other vinyl monomers [30–34]. Therefore, the incorporation of PNIPAAm into a β-CD-based hydrogel lead to an efficient biomaterial for "*smart*" delivery of anticancer drugs in respond to the thermal trigger.

The above-mentioned types of DDSs can be more fortify by the integration of magnetic nanoparticles (MNPs). Iron oxide NPs are the most common type of MNPs owing to their biocompatibility, low toxicity, as well as simple and inexpensive synthesis methods [35–38]. The advantages of a magnetic DDS can listed as isolation in the target area easily and rapidly by applying magnetic force, diagnosis by magnetic resonance imaging (MRI) approach, and hyperthermia therapy [39,40]. Hyperthermia is a potent cancer therapy strategy owing to its negligible side effects. Despite, the main disadvantage of this treatment approach are deficiency of heat distribution in all tumoral cells, the unavoidable delivery of heat to adjacent healthy cells, and the necessity for careful control of the patient's temperature and physiological situation during therapy process [41]. So, the hyperthermia therapy can be considered as an eficient strategy in association with chemotherapy to achieve better clinical outcomes [42–45].

According to the above-discussed facts, we hypothesize that a hydrogel containing β-CD, PNIPAAm, and Fe_3O_4 NPs can be act as a *de novo* thermal-responsive DDS for chemo- and hyperthermia-therapies of cancer. Furthermore, owing to amphiphilic nature of β-CD such system can be applied for delivering either hydrophobic and hydrophilic anticancer drugs or their combination with decreasing systematic toxicity of anticancer drugs. For this aim, β-CD was modified by maleic anhydride (MA) followed by copolymerization with *N*-isopropylacrylamide (NIPAAm) monomer and thiol-end capped Fe_3O_4 NPs through a free radical copolymerization technique. Ddoxorubicin hydrochloride (Dox) was physically loaded into the DDS as an anticancer agent, and drug encapsulation and loading capacities as well as thermal-stimulated Dox release behavior were examined. The cytocompatibility of the synthesized hydrogel was approved by MMT-assay. The cytotoxicity of the drug-loaded hydrogel was assessed using MCF7 cells *via* MTT-assay by chemotherapy, hyperthermia therapy as well as combination chemo/hyperthermia therapy.

2. Experimental

2.1. Materials

The monomer (*N*-isopropylacrylamide; NIPAAm) was purchased from Sigma-Aldrich (St. Louis, MO, USA) and re-crystallized from *n*-hexane/toluene mixture (90/10 v/v) for purification. β-Cyclodextrin (β-CD) was acquired from Sigma-Aldrich, re-crystallized from hot water, and then dried. Ferric chloride hexahydrate ($FeCl_3.6H_2O$), ferrous chloride tetrahydrate ($FeCl_2.4H_2O$), *N*,*N*′-methylene-bis (acrylamide) (MBAm), NH_4OH (25 % of ammonia), maleic anhydride (MA), *N*,*N*-dimethylformamide (DMF), *N*,*N*,*N*′,*N*′-tetramethylethylenediamine (TEMED), and 3-(trimethoxysilyl)-1-propanethiol were obtained from Sigma-Aldrich. Fetal bovine serum (FBS), phosphate buffered saline (PBS), and MTT (3-(4,5-dimethylthiazol-2-yl)-2,5-diphe-nyltetrazolium bromide) were achieved from Invitrogen (Carlsbad, CA, USA). The MCF7 cell line (NCBI Code: C135) was provided from national cell bank of Iran (Pasteur Institute, Tehran, Iran).

2.2. Synthesis of β-CD-MA

A 100-mL reaction vessel was charged with β-CD (2.30 g, 2 mmol) and distilled DMF (30 mL). The content was de-aerated by argon gas for some minutes, followed by adding hexane washed NaH (0.40 g, 16.80 mmol). The content was disturbed for about 2 h, and then added MA (1.00 g, in 10 mL of dried DMF). After stirring for about 1 h, the temperature was raised to 45 °C. The flask's content was disturbed for 13 h followed by precipitation in a acetone (400 mL) [46]. The product obtained was vacuum-dried overnight (Yield: 2.17 g).

2.3. Synthesis of thiol end-capped MNPs

The Fe_3O_4 NPs were produced by the well-established co-precipitation technique. For this objective, a solution composed of $FeCl_2$

(30 mL, 0.3 molL^{-1}) and $FeCl_3$ (60 mL, 0.3 molL^{-1}) was transferred in to a 250-mL reactor. The reaction mixture was de-aerated by purging argon for 15 min, followed by heating up to 80 ± 3 °C. Subsequently, NH_4OH solution (25 mL) was dropped to the reactor under stirring at inert atmosphere. At the end of process, the mixture was disturbed for additional 1 h at 80 ± 3 °C followed by cooling through the removing of flask from oil bath. The black MNPs were precipitated by centrifugation at 5000 rpm, and then washed using deionized water and ethanol till its pH becomes neutral. The obtained black powder was dried in vacuum [47].

The MNPs surface's were modified by 3-(trimethoxysilyl)-1-propanethiol as follows. The synthesized MNPs (1.20 g) were dispersed in ethanol (70 mL) by means of sonication. After that, 3-(trimethoxysilyl)-1-propanethiol (1.50 mL, 8.00 mmol) was added slowly to the reactor under stirring. The content was disturbed for 15 h at 70 ± 3 °C. The synthesized 3-(trimethoxysilyl)-1-propanethiol-modified MNPs were collected by centrifugation at 5000 rpm. After this, the NPs were re-dispersed in ethanol (150 mL), disturbed for 4 h followed by centrifugation to remove by-products and un-reacted 3-(trimethoxysilyl)-1-propanethiol. The final product was obtained after vacuum-drying as black powder [18].

2.4. Synthesis of β-CD-g-PNIPAAm/Fe_3O_4 magnetic hydrogel

The thermal-responsive magnetic hydrogel based on β-CD (β-CD-*g*-PNIPAAm/Fe_3O_4) was produced *via* a free radical copolymerization of β-CD-MA multi-functional macromonomer, NIPAAm monomer, and thiol-end capped Fe_3O_4 NPs in the presence of a crosslinker (MBAm) and an accelerator (TEMED). A 100-mL reaction vessel was charged with β-CD-MA (1.00 g; 0.60 mmol), NIPAAm monomer (1.50 g; 13.2 mmol), 3-(trimethoxysilyl)-1-propanethiol-modified MNPs (100 mg), MBAm (65 mg; 0.043 mmol), TEMED (40 μL; 0.044 mmol), and distilled water (50 mL). The mixture was de-oxygenated using argon gas for 15 min followed by adding KPS (70 mg; 0.26 mmol) as radical initiator. Afterward, the flask was warmed up to 60 ± 3 °C through placing in an oil bath, and the content was disturbed for 18 h under argon protection. So, the crude product was immersed into distilled water (400 mL) for two days by refreshing the water each 10 h to remove the by-products and remaining monomer [48,49]. The pure product was isolated by lyophilizing (Yield: 2.37 g).

2.5. Sol and gel fractions

The as-produced β-CD-*g*-PNIPAAm/Fe_3O_4 hydrogel was dried at 40 ± 3 °C. The hydrogel was weighed each 24 h until the mass variation was <0.1 mg in any 24 h (labelled as M_1). A Soxhlet tool with distilled water as the eluent was used to extract the sol fraction of the magnetic hydrogel. The hydrogel was then dried till there is no noteworthy mass alteration (labelled as M_2). The sol and gel fractions (%) of the sample were quantified by the following equations [50].

$$\text{Sol fraction } (\%) = \frac{(M_1 - M_2)}{M_1} \times 100$$

Gel fraction (%) = 1- sol fraction.

2.6. Dox formulation

The β-CD-*g*-PNIPAAm/Fe_3O_4-Dox was fabricated by mixing of hydrogel and Dox in an aqueous media. In brief, a 50-mL flask was charged with the β-CD-*g*-PNIPAAm/Fe_3O_4 (300 mg), Dox (30 mg), and distilled water (35 mL). The flask content was disturbed at ambient condition for 24 about hours. Subsequently, the content was filtered, and drug encapsulation (EE) and loading (LE) efficiencies were measured from calibration curve *via* the analyzing of supernatant by UV–vis spectroscopy at 480 nm by following equations [51].

$$EE = \frac{\textit{Amount of Dox loaded}}{\textit{Initial amount of Dox added}} \times 100$$

$$LE = \frac{\textit{Amount of Dox loaded}}{\textit{Mass of Polymer}} \times 100$$

2.7. In vitro drug release assessment

The thermal-responsiveness release of Dox from the fabricated β-CD-*g*-PNIPAAm/Fe_3O_4-Dox was approved through the studding *in vitro* drug release behavior at 37 and 40 °C. Briefly, the β-CD-*g*-PNIPAAm/Fe_3O_4-Dox was dissolved in PBS (15 mL, 0.1 molL^{-1}), transferred into a dialyze membrane bag with a molecular weight cut-off of 14 KDa. The bag containing β-CD-*g*-PNIPAAm/Fe_3O_4-Dox was dialyzed against PBS solution (0.10 molL^{-1}) at 37 and 40 °C (pH 7.4). At predetermined times, 1.00 mL of release media was took out from the beaker and the amount of released drug was measured using UV–vis spectrophotometry [52].

2.8. In vitro cytotoxicity studies

2.8.1. Chemotherapy

The cytocompatibility of the β-CD-*g*-PNIPAAm/Fe_3O_4 and cytotoxicity of drug-loaded hydrogel were surveyed using MCF7 cells by

the MTT-assay. Briefly, the MCF7 cells were cultured in RPMI1640 media having antibiotic (100 UmL^{-1} streptomycin and 100 UmL^{-1} penicillin) followed by supplementation with FBS (10 % v/v). The MCF7 cells (5.0×10^3 cells per well) were then incubated in a humidified incubator at 37 °C with 5 % CO_2. The growth media refreshed each two days. The MCF7 cells was then isolated, seeded in a 96-well plate followed by incubation for 24 h. Subsequently, the MCF7 cells were exposed for 24 and 48 h with different concentrations (2, 4, 6, and 10 μgmL^{-1}) of β-CD-*g*-PNIPAAm/Fe_3O_4-Dox (based on Dox concentration) and free Dox. Subsequently, the culture medium containing drug was replaced with a fresh MTT solution (50 μL) and growth media (150 μL) followed by incubation for additional 4 h. After that, the residual MTT solution was removed, dimethyl sulfoxide (DMSO; 200 μL) possess 25 μL of Sorenson's buffer was added to each well to dissolve formazan crystals.

Finally, the viability of MCF7 cells was investigated using spectroscopy approach at 570 nm by means of a spectrophotometric plate reader (ELx 800, Biotek, San Francisco, CA, USA) [53].

$$\text{Cell viability } (\%) = \frac{A_{570\ (sample)}}{A_{570\ (control)}} \times 100$$

2.8.2. Chemo/hyperthermia therapy

Cytotoxicity of the developed DDS was also examined in synergistic chemo/hyperthermia therapy. The process was completed as above-mentioned procedure, only at last 2 h the test tubes were immersed in water at 45 °C to examine the chemo/hyperthermia therapy efficiency of the β-CD-*g*-PNIPAAm/Fe_3O_4-Dox [28].

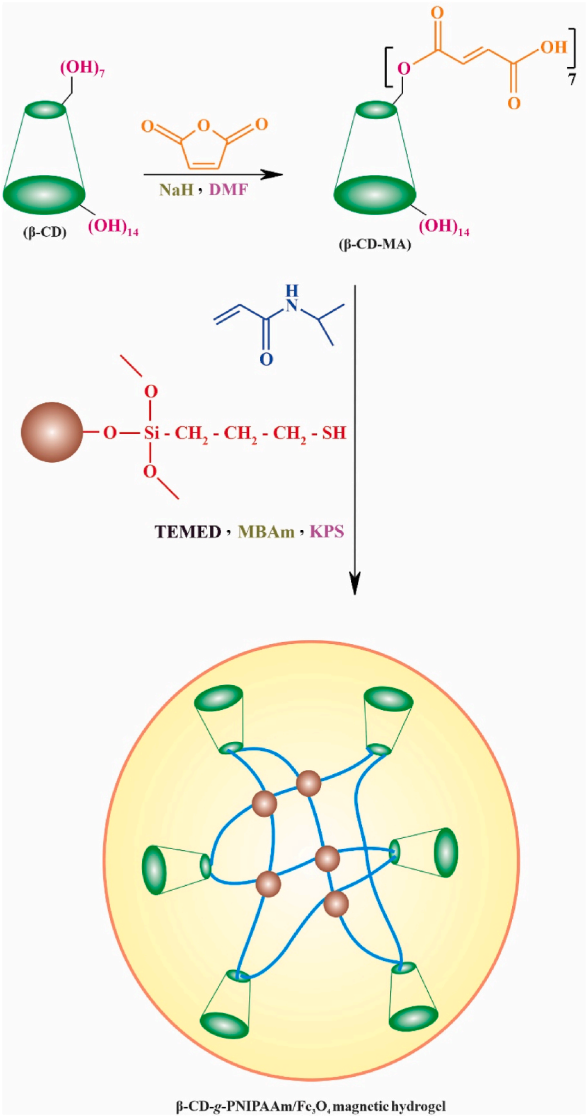

Scheme 1. The synthesis strategy for β-CD-*g*-PNIPAAm/Fe_3O_4 magnetic hydrogel.

2.8.3. In vitro cellular uptake

For the evaluation of cellular uptake, the cancerous cells were seeded in a 12-well plate (4.0×10^5 cells per well) and after 24 h, the complete mediums were removed, and instead the cells were exposed with Dox and Dox-loaded β-CD-*g*-PNIPAAm/Fe_3O_4 magnetic hydrogel. After 6 h, the treatment media was removed, the cells were washed with PBS, meticulously followed by detaching using trypsin digestion. The suspended cells were centrifuged (600 rpm), the isolated cells were then suspended in PBS, and the percent of drug uptake was quantified in total events of 10.000 cells employing a Macsquant analyzer 10 flow cytometer (Miltenyi Biotec GmbH; Bergisch Gladbach, Germany) in an appropriate band-pass filter (Excitation: 470 nm, Emission 595 nm) [54].

2.9. Characterization

Fourier transform infrared (FTIR) spectra of the samples were collected on a Shimadzu 8101 M FTIR (Kyoto, Japan) *via* pellet approach. Wavenumber resolution of 4 cm^{-1} as single scan in spectral range from 400 to 4000 cm^{-1} was selected for FTIR spectroscopy. Proton nuclear magnetic resonance (^{1}H NMR) spectra were provided on a FT-NMR, 400 MHz (Bruker Optik GmbH, Ettlingen, Germany) at room temperature. For NMR spectroscopy, samples (10 mg) were dissolved in deuterated solvent (1 mL; DMSO or water). Chemical shifts were reported in ppm by considering tetramethylsilane (TMS) as an internal reference. The spectra were provided with 20 scans. A scanning electron microscope (FEI Quanta 450, USA) was employed to study the surface morphologies of the products at 30.0 kV after coating the surface of samples with a thin layer of gold. A CM10-TH microscope (Philips, Eindhoven, The Netherlands) at a 100 kV accelerating voltage used for transmission electron microscopy (TEM) imaging. The sample for TEM imaging was prepared by suspension of hydrogel in ethanol (5 wt%) followed by sonication for 10 min and drop casting over a carbon-coated copper grid. The most portion of ethanol was adsorbed through touching the side of the grid by a filter paper, and then allowed to evaporate in ambient condition. Magnetic properties of the products were assessed using a vibrating sample magnetometer (VSM, MDKFT, Iran). Powder X-ray diffraction (XRD) analysis was recorded by a Siemens D5000 diffractometer (Aubrey, Texas, USA) possesses X-ray generator of a CuK_α radiation at $\lambda = 1.5406$ Å in the scan range from 10 to 70° (2θ). UV–vis spectroscopy was conducted on a Shimadzu 1650 PC equipment (Kyoto, Japan).

3. Results and discussion

It is a decisive fact that cancer is one of the leading health issues at current time. Chemo/hyperthermia treatment using multi-modal natural component-based magnetic hydrogels can be considered as an effective cancer treatment approach owing to their intrinsic biological/physicochemical characteristics, which lead to proper treatment outcomes [28]. So, the present study focused to design and fabrication a thermal-responsive magnetic hydrogel based on β-CD for chemo/hyperthermia therapy of cancerous cells (Scheme 1).

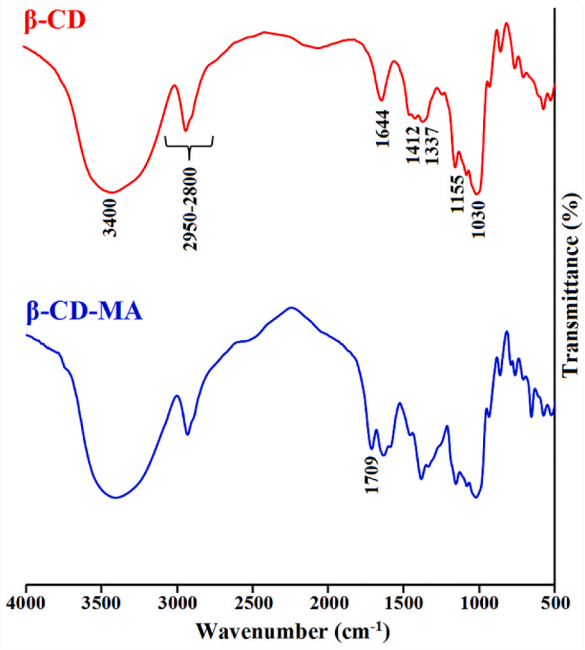

Fig. 1. The FTIR spectra of neat β-CD and β-CD-MA.

3.1. Characterization of β-CD-MA

The β-CD was functionalized by MA using an esterification reaction to induce vinyl groups for free radical polymerization. The successful synthesis was approved by FTIR and ^{1}H NMR spectroscopies as indicated in Figs. 1 and 2. The principal absorption bands of pure β-CD are the stretching vibrations of aliphatic C–H groups at 2950 to 2800 cm^{-1} region, the bending vibrations of aliphatic C–H groups at 1337 and 1412 cm^{-1}, the stretching vibrations of various C–O groups at 1030 and 1155 cm^{-1}, as well as the stretching and bending vibrations of primary and secondary hydroxyl (—OH) groups were observed at 1644 and 3400 cm^{-1}, respectively [55]. The successful modification of β-CD with MA was established over advent of a new adsorption band at 1709 cm^{-1} corresponded to the carbonyl group of MA as seen in Fig. 1.

The production of β-CD-MA was further proved by ^{1}H NMR spectroscopy as indicated in Fig. 2. In ^{1}H NMR spectrum of the neat β-CD the primary hydroxyl group (f) was observed at 4.90 ppm, while the secondary hydroxyl groups (h) were appeared at 5.95 and 5.85 ppm. The various C–H protons of the β-CD (a, b, c, d, and e) were witnessed at 3.20 to 3.80 ppm [55]. The advent of vinyl protons at 5.30 (n) and 6.60 (m) ppm confirm the successful functionalization of β-CD using MA. The chemical shift at 6.20 ppm (o) may be related to vinyl protons in the butenedioic diester groups between β-CD molecules [56]. In addition, the acetylation degree in the primary hydroxyl group was quantified as 79 % for monoester and 6.5 % for diester moieties using ^{1}H NMR data.

3.2. Characterization of β-CD-g-PNIPAAm/Fe_3O_4 magnetic hydrogel

3.2.1. FTIR spectroscopy

Surface of Fe_3O_4 NPs were modified using a silan coupling agent to improve their compatibility with organic matrix, prevent their aggregation as well as induction of thiol group. It should be pointed out that the thiol-end capped MNPs could provide "acrylamide–thiol" polymerization system, which progress *via* step-growth mechanism. In this polymerization approach, propagation and chain transfer alternate mechanism led to control of molecular weight of the resultant polymeric network [57,58]. The Fe_3O_4 NPs, thiol-end capped Fe_3O_4 NPs (Fe_3O_4-SH NPs), and β-CD-*g*-PNIPAAm/Fe_3O_4 hydrogel were analyzed by FTIR spectroscopy as indicated in Fig. 3. The FTIR spectrum of the Fe_3O_4 NPs displayed the characteristic stretching vibration of Fe–O at 571 cm^{-1}, and the hydroxyl's bending and stretching vibrations at 1598 and 3380 cm^{-1}, respectively. After surface modification of NPs with 3-(trimethoxysilyl)-1-propanethiol moiety the most significant variations are the advent of the stretching vibrations of C–H groups at 2950 to 2800 cm^{-1} region and slightly decreasing the intensity of stretching vibration of the hydroxyl groups at 3360 cm^{-1}.

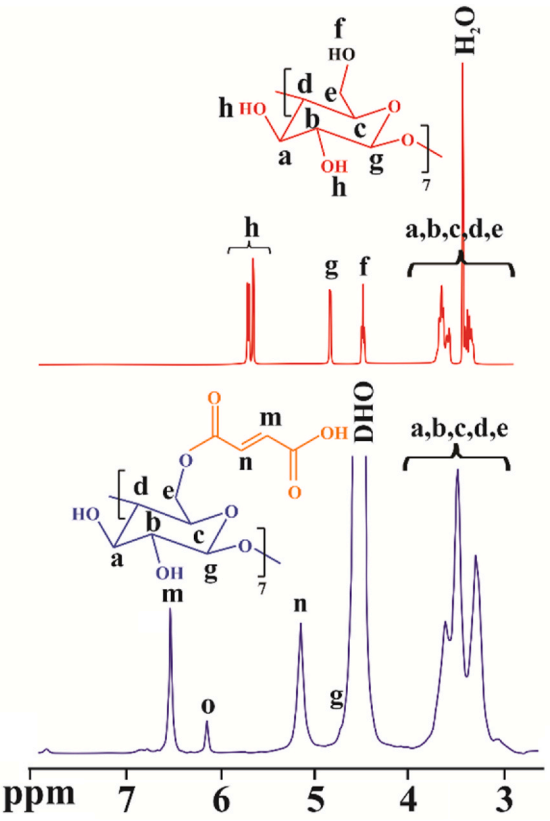

Fig. 2. The ^{1}H NMR spectra of the neat β-CD (in DMSO-d_6) and β-CD-MA (in D_2O).

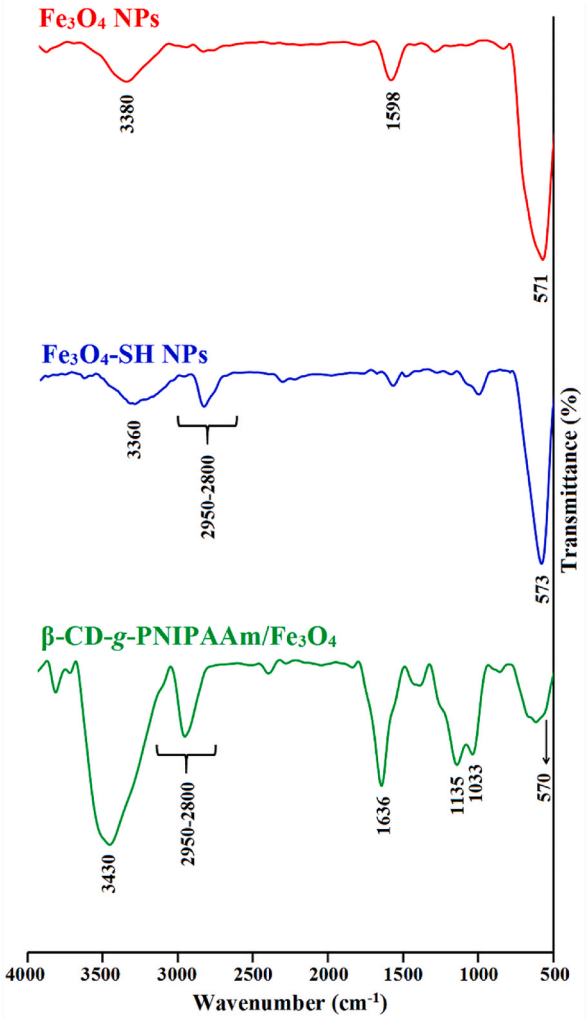

Fig. 3. The FTIR spectra of the Fe_3O_4 NPs, Fe_3O_4-SH NPs, and β-CD-*g*-PNIPAAm/Fe_3O_4 magnetic hydrogel.

The FTIR spectrum of the β-CD-*g*-PNIPAAm/Fe_3O_4 magnetic hydrogel showed the absorption bands related to the stretching vibrations of hydroxyl groups (associated to the Fe_3O_4 NPs and β-CD) as well as the stretching vibration of secondary N–H (associated to the amid group of PNIPAAm) as a robust and wide band at 3430 cm^{-1}, the stretching vibrations of various C–H groups at 2950 to 2800

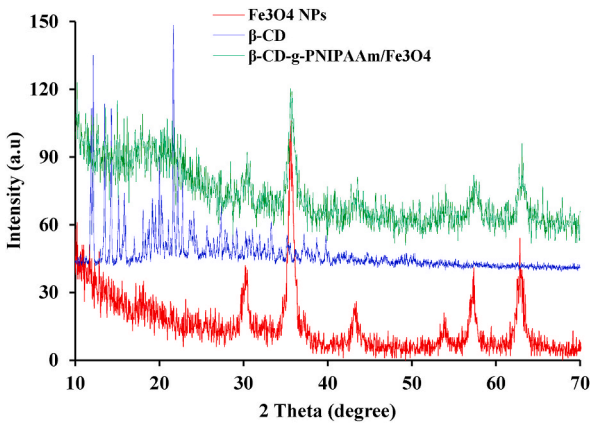

Fig. 4. The XRD patterns of Fe_3O_4 NPs, pure β-CD, and β-CD-*g*-PNIPAAm/Fe_3O_4 magnetic hydrogel.

cm^{-1} region, the stretching vibration of amide's carbonyl group at 1636 cm^{-1}, the stretching vibrations of various C–O groups (related to PNIPAAm and β-CD) at 1135 and 1033 cm^{-1}, and the stretching vibration of Fe–O at 570 cm^{-1}.

3.2.2. XRD patterns

The crystallinity of the MNPs, pure β-CD, and β-CD-*g*-PNIPAAm/Fe_3O_4 hydrogel were analyzed by XRD as indicated in Fig. 4. The XRD pattern of the pristine MNPs displayed some peaks at 2θ diffraction values of 2θ = 30.5°, 36.0°, 43.2°, 52.8°, 57.9°, and 63.0°

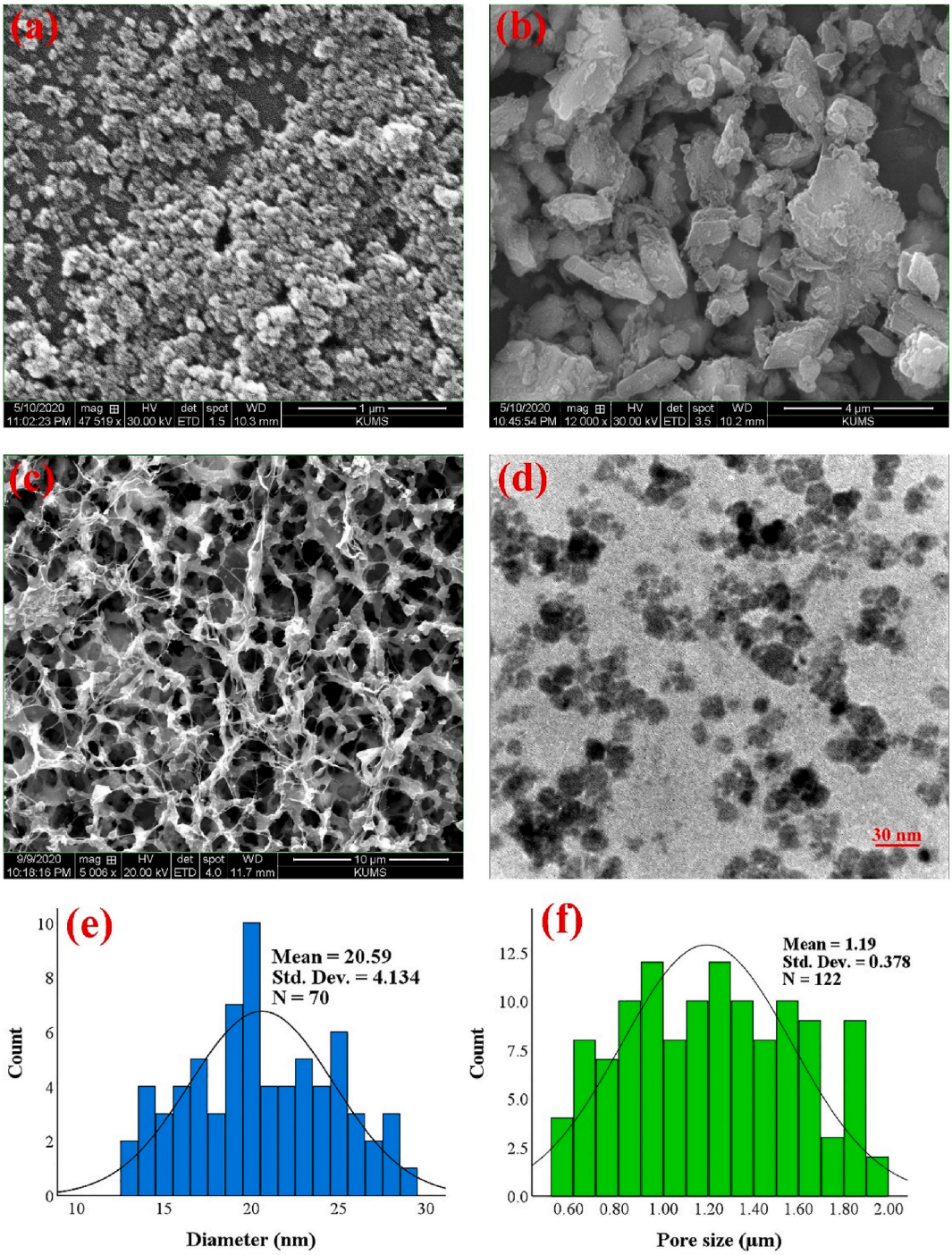

Fig. 5. The SEM images of the Fe_3O_4 NPs (a), pristine β-CD (b), and the SEM (c) and TEM (d) images of β-CD-*g*-PNIPAAm/Fe_3O_4 magnetic hydrogel, and the size distribution of NPs (e) and pore-size distribution of hydrogel (f).

conforming the (220), (311), (400), (422), (511) and (440) prisms of Fe_3O_4 crystalline structure, respectively [59]. As seen, the pure β-CD has crystalline structure (in polyhedral form). The most important peaks were appeared at 2θ diffraction values of 12.56°, 18.01°, 19.20°, 21.6°, 24.2°, 27.3° and 35.6°. All the diffraction peaks could be indexed to β-CD (JCPDS card 00-054-1476) [28,60]. The XRD patterns of the synthesized β-CD-*g*-PNIPAAm/Fe_3O_4 magnetic hydrogel displayed the diffraction peaks of Fe_3O_4 NPs, but reduced in their intensity, mainly due to the small amount of MNPs in the sample and the amorphous nature of PNIPAAm. Furthermore, the diffraction peaks of β-CD were covered by the broad peak of amorphous PNIPAAm.

3.2.3. Morphology study

The SEM micrographs of Fe_3O_4 NPs, pure β-CD, and SEM and TEM images of β-CD-*g*-PNIPAAm/Fe_3O_4 hydrogel as well as size distribution of NPs and pore-size distribution of hydrogel are indicated in Fig. 5. The SEM micrograph of the as-fabricated Fe_3O_4 NPs displayed spherical shape for the NPs. The average diameter of these NPs were estimated as 20.6 ± 4.1 nm (Fig. 5 **a** and **e**). The SEM micrograph of the pristine β-CD showed irregular particles shapes. The key reason for this is aggregation of β-CD molecules through strong physical interactions (*e.g.,* hydrogen bond among the hydroxyl groups) (Fig. 5**b**).

The SEM micrograph of the fabricated β-CD-*g*-PNIPAAm/Fe_3O_4 hydrogel showed a porous microstructure with pore-size distribution of 1.19 ± 0.37 μm (Fig. 5 **c** and **f**). The morphology of the developed β-CD-*g*-PNIPAAm/Fe_3O_4 hydrogel was more studied by TEM as depicted in Fig. 5**d**. In this image, dark regions represents Fe_3O_4 NPs, which homogenously dispersed in the hydrogel network. The most important explanations for this fact include the chemical modification of Fe_3O_4 NPs with 3-(trimethoxysilyl)-1-propanethiol, and subsequently the chemical bonding of modified Fe_3O_4 NPs to the hydrogel neatwork, as well as the robust physical interactions, including hydrogen bond among the polymeric network functionalities (*e.g.,* hydroxyl and carbonyl) and surface hydroxyl groups of Fe_3O_4 NPs.

3.2.4. Magnetic property study

The VSM equipment was applied to examine the magnetic features of the Fe_3O_4 NPs and β-CD-*g*-PNIPAAm/Fe_3O_4 hydrogel as presented in Fig. 6. The saturation magnetization (δ_s) for the Fe_3O_4 NPs and β-CD-*g*-PNIPAAm/Fe_3O_4 hydrogel were obtained as 49.6 and 8.2 emu g^{-1}, respectively.

3.3. Crosslinking efficiency

The crosslinking efficiency and stability of the produced β-CD-*g*-PNIPAAm/Fe_3O_4 hydrogel was examined by the assessing of its SF and GF values. The SF and GF values for the hydrogel were established as 23 ± 1.6 and 77 ± 1.6, respectively. As the literature, this value of GF represent acceptable crosslinking efficiency and stability for the β-CD-*g*-PNIPAAm/Fe_3O_4 magnetic hydrogel [50].

3.4. Calculation of LE and EE values

According to porous morphology of the developed β-CD-*g*-PNIPAAm/Fe_3O_4 hydrogel, it is expected that the sample exhibited adequate EE and LE values. Another parameter that may be affect the EE and LE amounts is physical interactions of drug molecules with numerous functional groups in the hydrogel network (*e.g.,* hydroxyl and carboxyl). The LE and EE values for the β-CD-*g*-PNIPAAm/Fe_3O_4 hydrgel were obtained as 7.3 ± 0.24 and 73 ± 2.4 %, respectively.

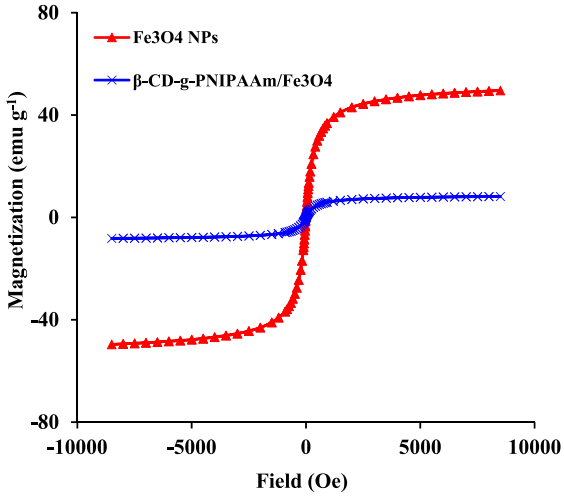

Fig. 6. The magnetization curves of the Fe_3O_4 NPs and β-CD-*g*-PNIPAAm/Fe_3O_4 hydrogel.

3.5. Drug release assessment

The Dox release profile of the β-CD-*g*-PNIPAAm/Fe_3O_4-Dox was assessed under thermal-triggered condition (Fig. 7). The free Dox has a speedy and complete dissolution due to its great solubility in the dissolution media. Moreover, temperature has a tiny role on the release behavior of the free Dox. For the β-CD-*g*-PNIPAAm/Fe_3O_4-Dox, in physiological condition the sample represent relatively low drug release value due to strong hydrogen bonds between the Dox molecules and the hydrogel network. By contrast, through increasing temperature up to 40 °C the release amount was improved sensationally owing to collapse of PNIPAAm chains. However, the release of Dox from the fabricated magnetic hydrogel is slow, and at first 24 h, only 33.8 % of loaded Dox was released at mentioned condition. As the literature, the tumors have abnormal micro-environment (*e.g.,* higher temperature value than those of the normal tissues), so, the developed β-CD-*g*-PNIPAAm/Fe_3O_4-Dox has potential for controlled and targeted delivery of anticancer drugs to the cancer sites [53].

3.6. Release-rate kinetic

As the importance role of drug release kinetic in drug delivery purposes, the *in vitro* drug release data were studied *via* numerous kinetic models (*e.g.,* zero order, first order, Higuchi, Hixon-Crowell, and Korsmeyer-Peppas) [61]. The most important parameters that influence the release kinetic are matrix materials properties (*e.g.,* swelling and degradation), drug compounds and its physicochemical properties (*e.g.,* solubility, charge, and interaction with matrix) and release media feature (*e.g.,* pH, temperature, enzyme, and ionic strength) [27].

The coefficient of determination (R^2) for the β-CD-*g*-PNIPAAm/Fe_3O_4-Dox at temperature values of 37 and 40 °C were determined (Table 1). As the results, the release of free Dox in both situations fitted with first-order model. So, the release rate of free Dox is concentration-dependent process. The release data of the β-CD-*g*-PNIPAAm/Fe_3O_4-Dox were kinetically best fitted with the Higuchi model. The R^2 in this kinetic model was higher than other models in both conditions, indicating the release of drug from β-CD-*g*-PNIPAAm/Fe_3O_4-Dox is principally controlled by diffusion mechanism [52].

3.7. Biological tests

3.7.1. Cytocompatibility

The first prerequisite for the *in vivo* usage of a biomaterial is its cytocompatibility. Therefore, we investigated this requirement using MTT-assay and the results are depicted in Fig. 8**a**. As illustrated, the fabricated β-CD-*g*-PNIPAAm/Fe_3O_4 hydrogel represent acceptable cytocompatibility. In fact, the fabricated sample showed proper cell viability (95.3 %) even at high concentration (40 mg mL^{-1}).

3.7.2. In vitro anticancer activity

The cytotoxicity of the β-CD-*g*-PNIPAAm/Fe_3O_4-Dox was assayed using MCF7 cells *via* both chemotherapy and chemo/hyperthermia therapy by the well-known MTT-assay (Fig. 8**b** and **c**). Free Dox represent greater anticancer efficiency than the β-CD-*g*-PNIPAAm/Fe_3O_4-Dox in both chemotherapy and chemo/hyperthermia therapy during 24 h, mainly due to burst obtainability of free Dox in a tiny time against sustained Dox release nature of the β-CD-*g*-PNIPAAm/Fe_3O_4-Dox and low effectiveness of hyperthermia therapy. However, the free Dox has not recommended owing to its some disadvantages such as fast drug clearance, weak drug biodistribution, and importantly systemic toxicity. Furthermore, employing combination of chemotherapy and hyperthermia therapy displayed slightly greater anticancer activity than the chemotherapy alone (Fig. 8**b**).

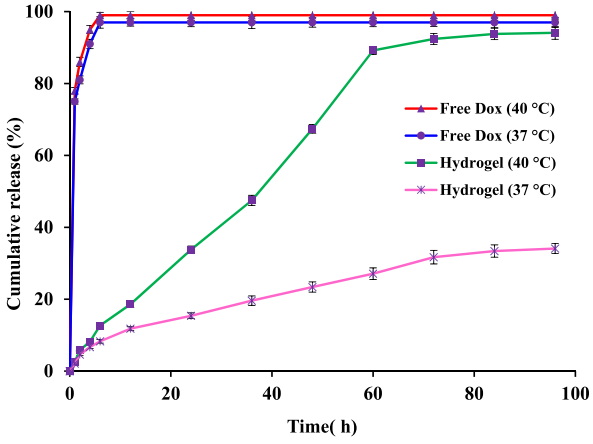

Fig. 7. *In vitro* drug release results of the β-CD-*g*-PNIPAAm/Fe_3O_4-Dox at temperature values of 37 and 40 °C (PBS; pH 7.4). All experiment were performed in triplicate.

Table 1
The release kinetic study results of β-CD-*g*-PNIPAAm/Fe_3O_4-Dox and free Dox.

Model name	β-CD-*g*-PNIPAAm/Fe_3O_4-Dox (R^2)		Free Dox (R^2)	
	37 °C	40 °C	37 °C	40 °C
Zero-order $C_t = C_0 + K_0t$	0.71	0.75	0.72	0.78
Fist-order $DC/dt = -K_1C$	0.82	0.85	0.91	0.94
Hixson-Crowell $(100\text{-}Q_t)^{1/3} = 100^{1/3} - k_{HC}.t$	0.83	0.86	0.73	0.77
Higuchi $Q_t = k_H.t^{1/2}$	0.93	0.95	0.79	0.82
Korsmeyer-Peppas $M_t/M\infty = K_{kp}t^n$	0.79	0.82	0.41	0.43

After 48 h treatment (Fig. 8**c**), the β-CD-*g*-PNIPAAm/Fe_3O_4-Dox represent greater anticancer activity than the free Dox in all concentrations of drug. Moreover, it was established that the chemo/hyperthermia therapy has synergistic effect on anticancer activity of the DDS.

3.8. In vitro cellular uptake

The *in vitro* cellular uptake was studied to approve the higher accumulation of released Dox in MCF7 from drug-loaded β-CD-*g*-PNIPAAm/Fe_3O_4 magnetic hydrogel in comparison to free Dox. The intrinsic fluorescent feature of Dox was employed for the quantification of the percent of drug uptake. The flow cytometry analyses showed greater cellular uptake of Dox in the cells treated with Dox-loaded β-CD-*g*-PNIPAAm/Fe_3O_4 magnetic hydrogel (~70 %) compared to free Dox (~28 %), indicating increased and enhanced translocation of Dox-loaded β-CD-*g*-PNIPAAm/Fe_3O_4 magnetic hydrogel across the cells wall and accumulation in the cells (Fig. 9a and b and c).

4. Conclusions

A magnetic hydrogel-based thermal-responsive drug delivery system (DDS) contaning β-cyclodextrin (β-CD), poly(*N*-isopropylacrylamide) (PNIPAAm), and Fe_3O_4 nanoparticles (NPs) was designed and fabicated through "acrylamide-thiol" polymerization sysytem. The morphology study by SEM equpment revealed that the fabricated magnetic hydrogel possess porous nanostructure witought microphase separation owing the exccelnt compatibility of β-CD and PNIPAAm. The uniform and well-dispersion of MNPs with spherical shape throughout the hydrogel network, was estabilished by TEM analysis. The saturation magnetization (δ_s) of the synthesized β-CD-*g*-PNIPAAm/Fe_3O_4 hydrogel was found to be 8.2 emu g^{-1} by means of VSM equpment.

The sustained as well as thermal-triggered release profile of the developed DDS was confirmed through dialysis approach. According to kinetic studies, the release of Dox from developed DDS was best fitted with the Higuchi model, demonstrating the release of drug from β-CD-*g*-PNIPAAm/Fe_3O_4-Dox was chiefly controlled by diffusion mechanism. Cytotoxicity experiments through MTT-assay revelaed that the fabricated DDS has high cytocompatibility. While, the Dox-loaded β-CD-*g*-PNIPAAm/Fe_3O_4 displayed better anticancer performance than the free drug on MCF7 cells. It was established that during 48 h the association of chemo- and hyperthermia-therapies resulted to higher anticancer efficiency than the free drug. Taking together, the physicochemical as well as biological findings demonstrated that the fabricated β-CD-*g*-PNIPAAm/Fe_3O_4 magnetic hydrogel is a promising DDS for chemo/hyperthermia treatment of solid tumors. In author opinion, the developed hydrogel can be used as an implantable DDS for efficient chemo/hyperthermia treatment of solid tumors.

Declaration

The authors report no competing fnancial interest.

CRediT authorship contribution statement

Morteza Eskandani: Writing – review & editing, Software, Data curation. **Rana Jahanban-Esfahlan:** Writing – review & editing, Investigation, Data curation. **Mohammd Mehdi Sadughi:** Writing – review & editing, Software, Formal analysis. **Mehdi Jaymand:** Writing – review & editing, Writing – original draft, Supervision, Project administration, Methodology, Investigation, Funding acquisition, Formal analysis, Data curation, Conceptualization.

Declaration of competing interest

The authors declare that they have no known competing financial interests or personal relationships that could have appeared to influence the work reported in this paper.

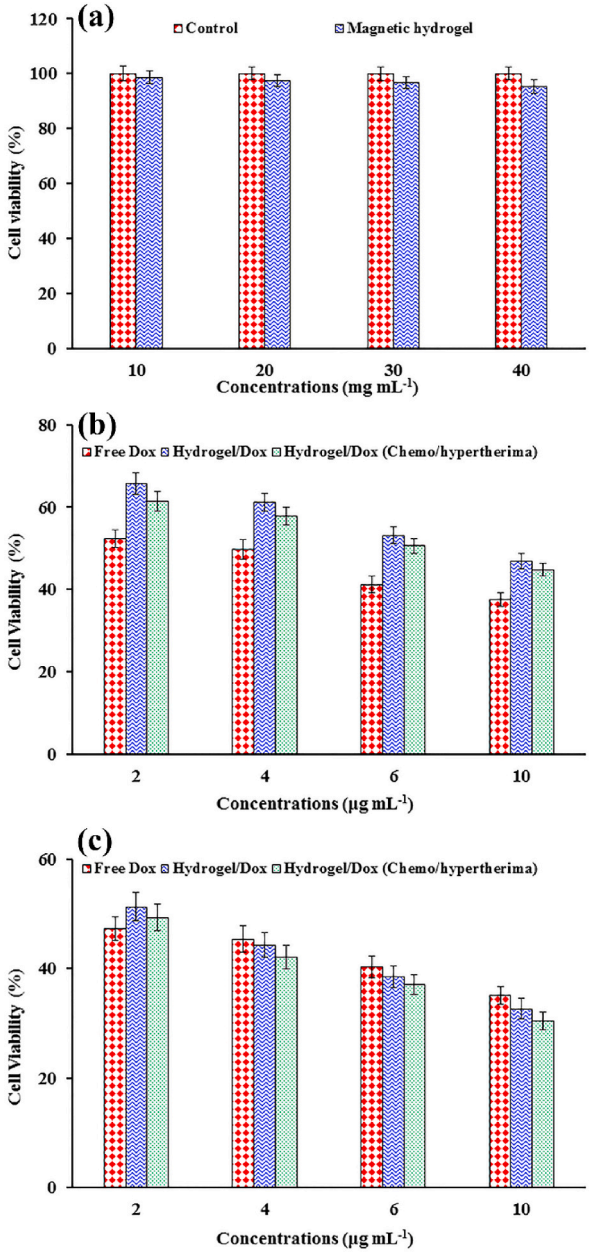

Fig. 8. The cytocompatibility of the β-CD-*g*-PNIPAAm/Fe_3O_4 magnetic hydrogel against MCF7 cells during 24 h (a), and cytotoxicity results of β-CD-*g*-PNIPAAm/Fe_3O_4-Dox in chemotherapy and chemo/hyperthermia therapy, and free Dox on MCF7 cells during 24 (b) and 48 (c) hours using MTT-assay (All experiment were performed in triplicate).

SPSS results ($p < 0.05$: considered statistically significant differences): In Fig. 8a: Data are not shown statistically significant differences ($p > 0.05$). In Fig. 8b: In 2 μg mL^{-1}: free Dox/hydrogel-Dox (chemotherapy): $p = 0.035$; free Dox/hydrogel-Dox (chemo/hyperthermia): $p = 0.039$; hydrogel-Dox (chemotherapy)/hydrogel-Dox (chemo/hyperthermia): $p = 0.047$. In 4 μg mL^{-1}: free Dox/hydrogel-Dox (chemotherapy): $p = 0.037$; free Dox/hydrogel-Dox (chemo/hyperthermia): $p = 0.041$; hydrogel-Dox (chemotherapy)/hydrogel-Dox (chemo/hyperthermia): $p = 0.051$. In 6 μg mL^{-1}: free Dox/hydrogel-Dox (chemotherapy): $p = 0.036$; free Dox/hydrogel-Dox (chemo/hyperthermia): $p = 0.044$; hydrogel-Dox (chemotherapy)/hydrogel-Dox (chemo/hyperthermia): $p = 0.058$. In 10 μg mL^{-1}: free Dox/hydrogel-Dox (chemotherapy): $p = 0.034$; free Dox/hydrogel-Dox (chemo/hyperthermia): $p = 0.042$; hydrogel-Dox (chemotherapy)/hydrogel-Dox (chemo/hyperthermia): $p = 0.063$. In Fig. 8c: In 2 μg mL^{-1}: free Dox/hydrogel-Dox (chemotherapy): $p = 0.046$; free Dox/hydrogel-Dox (chemo/hyperthermia): $p = 0.048$; hydrogel-Dox (chemotherapy)/hydrogel-Dox (chemo/hyperthermia): $p = 0.053$. In 4 μg mL^{-1}: free Dox/hydrogel-Dox (chemotherapy): $p = 0.067$; free Dox/hydrogel-Dox (chemo/hyperthermia): $p = 0.046$; hydrogel-Dox (chemotherapy)/hydrogel-Dox (chemo/hyperthermia): $p = 0.053$. In 6 μg mL^{-1}: free Dox/hydrogel-Dox (chemotherapy): $p = 0.057$; free Dox/hydrogel-Dox (chemo/hyperthermia): $p = 0.043$; hydrogel-Dox (chemotherapy)/hydrogel-Dox (chemo/hyperthermia): $p = 0.051$. In 10 μg mL^{-1}: free Dox/hydrogel-Dox (chemotherapy): $p = 0.051$; free Dox/hydrogel-Dox (chemo/hyperthermia): $p = 0.041$; hydrogel-Dox (chemotherapy)/hydrogel-Dox (chemo/hyperthermia): $p = 0.048$.

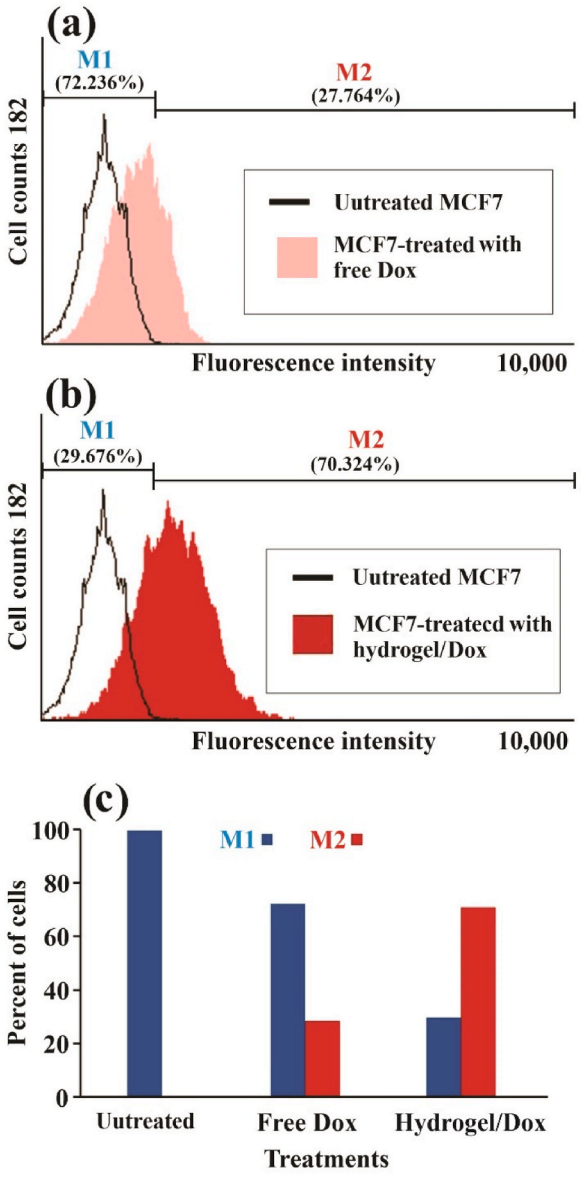

Fig. 9. Cellular uptakes of free Dox (a) and the Dox-loaded β-CD-*g*-PNIPAAm/Fe_3O_4 magnetic hydrogel in MCF7 cells using FACS flow cytometry (b), and cellular uptakes quantification of samples (c) (M1: fluorescent cells and M2: non-fluorescent cells; the fluorescent nature was obsrved through the internalization of Dox as a fluorescent drug).

Acknowledgements

This work was supported by Research Council of Kermanshah University of Medical Sciences, Kermanshah, Iran (Grant Number: 990464), and Students Research Committee, Kermanshah University of Medical Sciences, Kermanshah, Iran.

References

[1] D.M. Parkin, et al., Global cancer statistics, 2002, Ca-Cancer J. Clin. 55 (2) (2005) 74–108.
[2] T. Reya, et al., Stem cells, cancer, and cancer stem cells, Nature 414 (6859) (2001) 105–111.
[3] A. Mantovani, et al., Cancer-related inflammation, Nature 454 (7203) (2008) 436–444.
[4] A. Jemal, et al., Cancer statistics, 2006, Ca-Cancer J. Clin. 56 (2) (2006) 106–130.
[5] D. Peer, et al., Nanocarriers as an emerging platform for cancer therapy, Nat. Nanotechnol. 2 (12) (2007) 751–760.
[6] R.L. Siegel, K.D. Miller, A. Jemal, Cancer statistics, 2019, CA A Cancer J. Clin. 69 (1) (2019) 7–34.
[7] D.E.J.G.J. Dolmans, D. Fukumura, R.K. Jain, Photodynamic therapy for cancer, Nat. Rev. Cancer 3 (5) (2003) 380–387.
[8] M. Ferrari, Cancer nanotechnology: opportunities and challenges, Nat. Rev. Cancer 5 (3) (2005) 161–171.
[9] J.P. Stein, et al., Radical cystectomy in the treatment of invasive bladder cancer: long-term results in 1,054 patients, J. Clin. Oncol. 19 (3) (2001) 666–675.

[10] K.D. Miller, et al., Cancer treatment and survivorship statistics, 2016, CA A Cancer J. Clin. 66 (4) (2016) 271–289.
[11] M. Vallet-Regí, E. Ruiz-Hernández, Bioceramics: from bone regeneration to cancer nanomedicine, Adv. Mater. 23 (44) (2011) 5177–5218.
[12] R.K. Jain, T. Stylianopoulos, Delivering nanomedicine to solid tumors, Nat. Rev. Clin. Oncol. 7 (11) (2010) 653–664.
[13] J. Shi, et al., Cancer nanomedicine: progress, challenges and opportunities, Nat. Rev. Cancer 17 (1) (2017) 20–37.
[14] R. Duncan, Polymer conjugates as anticancer nanomedicines, Nat. Rev. Cancer 6 (9) (2006) 688–701.
[15] J. Li, X.J. Loh, Cyclodextrin-based supramolecular architectures: syntheses, structures, and applications for drug and gene delivery, Adv. Drug Deliv. Rev. 60 (9) (2008) 1000–1017.
[16] C. He, S.W. Kim, D.S. Lee, In situ gelling stimuli-sensitive block copolymer hydrogels for drug delivery, J. Contr. Release 127 (3) (2008) 189–207.
[17] J. Li, D.J. Mooney, Designing hydrogels for controlled drug delivery, Nat. Rev. Mater. 1 (12) (2016).
[18] A. Parvaresh, et al., Redox-and pH-responsive alginate-based magnetic hydrogel:“Smart” drug delivery and protein corona studies, J. Mol. Liq. 382 (2023) 121990.
[19] M. Jaymand, Chemically modified natural polymer-based theranostic nanomedicines: are they the golden gate toward a de novo clinical approach against cancer? ACS Biomater. Sci. Eng. 6 (1) (2019) 134–166.
[20] V.S. Ghorpade, A.V. Yadav, R.J. Dias, Citric acid crosslinked cyclodextrin/hydroxypropylmethylcellulose hydrogel films for hydrophobic drug delivery, Int. J. Biol. Macromol. 93 (2016) 75–86.
[21] P.L. Chee, et al., Supramolecular cyclodextrin pseudorotaxane hydrogels: a candidate for sustained release? Mater. Sci. Eng. C 39 (1) (2014) 6–12.
[22] Q. Yang, et al., Light-switchable self-healing hydrogel based on host–guest macro-crosslinking, Macromol. Rapid Commun. 38 (6) (2017).
[23] L. Dong, et al., Adaptive liquid microlenses activated by stimuli-responsive hydrogels, Nature 442 (7102) (2006) 551–554.
[24] B. Jeong, A. Gutowska, Lessons from nature: stimuli-responsive polymers and their biomedical applications, Trends Biotechnol. 20 (7) (2002) 305–311.
[25] M.A. Ward, T.K. Georgiou, Thermoresponsive polymers for biomedical applications, Polymers 3 (3) (2011) 1215–1242.
[26] I. Tokarev, S. Minko, Stimuli-responsive hydrogel thin films, Soft Matter 5 (3) (2009) 511–524.
[27] F. Mahmoodzadeh, et al., A novel gold-based stimuli-responsive theranostic nanomedicine for chemo-photothermal therapy of solid tumors, Mater. Sci. Eng. C 93 (2018) 880–889.
[28] M. Eskandani, et al., Folate-conjugated pH-and redox-responsive magnetic hydrogel based on tragacanth gum for “smart” chemo/hyperthermia treatment of cancerous cells, J. Drug Deliv. Sci. Technol. 84 (2023) 104449.
[29] H. Derakhshankhah, et al., Folate-conjugated thermal-and pH-responsive magnetic hydrogel as a drug delivery nano-system for “smart” chemo/hyperthermia therapy of solid tumors, Mater. Today Commun. 30 (2022) 103148.
[30] D. Schmaljohann, Thermo- and pH-responsive polymers in drug delivery, Adv. Drug Deliv. Rev. 58 (15) (2006) 1655–1670.
[31] C.M. Schilli, et al., A new double-responsive block copolymer synthesized via RAFT polymerization: poly(N-isopropylacrylamide)-block-poly(acrylic acid), Macromolecules 37 (21) (2004) 7861–7866.
[32] P. Eskandari, et al., Controlled release of anti-cancer drug from the shell and hollow cavities of poly(N-isopropylacrylamide) hydrogel particles synthesized via reversible addition-fragmentation chain transfer polymerization, Eur. Polym. J. 135 (2020).
[33] M. Haqani, H. Roghani-Mamaqani, M. Salami-Kalajahi, Synthesis of dual-sensitive nanocrystalline cellulose-grafted block copolymers of N-isopropylacrylamide and acrylic acid by reversible addition-fragmentation chain transfer polymerization, Cellulose 24 (5) (2017) 2241–2254.
[34] S. Hajebi, et al., Temperature-responsive poly(N-isopropylacrylamide) nanogels: the role of hollow cavities and different shell cross-linking densities on doxorubicin loading and release, Langmuir 36 (10) (2020) 2683–2694.
[35] X. Zhao, et al., Chitosan derived glycolipid nanoparticles for magnetic resonance imaging guided photodynamic therapy of cancer, Carbohydr. Polym. 245 (2020).
[36] F. Zhang, et al., Magnetic nanoparticles coated with polyphenols for spatio-temporally controlled cancer photothermal/immunotherapy, J. Contr. Release 326 (2020) 131–139.
[37] J. Liao, H. Huang, Smart pH/magnetic sensitive Hericium erinaceus residue carboxymethyl chitin/Fe3O4 nanocomposite hydrogels with adjustable characteristics, Carbohydr. Polym. 246 (2020).
[38] A. Jafarizad, et al., PEGylated graphene oxide/Fe 3O 4 nanocomposite: synthesis, characterization, and evaluation of its performance as de novo drug delivery nanosystem, Bio Med. Mater. Eng. 29 (2) (2018) 177–190.
[39] S. Laurent, et al., Magnetic iron oxide nanoparticles: synthesis, stabilization, vectorization, physicochemical characterizations and biological applications, Chem. Rev. 108 (6) (2008) 2064–2110.
[40] T. Neuberger, et al., Superparamagnetic nanoparticles for biomedical applications: possibilities and limitations of a new drug delivery system, J. Magn. Magn Mater. 293 (1) (2005) 483–496.
[41] M. Jaymand, Hydrogel-based drug delivery systems for synergistic chemo/hyperthermia therapy of cancer: a comprehensive review, J. Drug Deliv. Sci. Technol. (2024) 105581.
[42] R. Di Corato, et al., Combining magnetic hyperthermia and photodynamic therapy for tumor ablation with photoresponsive magnetic liposomes, ACS Nano 9 (3) (2015) 2904–2916.
[43] P. Diagaradjane, et al., Modulation of in vivo tumor radiation response via gold nanoshell-mediated vascular-focused hyperthermia: characterizing an integrated antihypoxic and localized vascular disrupting targeting strategy, Nano Lett. 8 (5) (2008) 1492–1500.
[44] C.L. Dennis, et al., Nearly complete regression of tumors via collective behavior of magnetic nanoparticles in hyperthermia, Nanotechnology 20 (39) (2009).
[45] H. Derakhshankhah, et al., A bio-inspired gelatin-based pH-and thermal-sensitive magnetic hydrogel for in vitro chemo/hyperthermia treatment of breast cancer cells, J. Appl. Polym. Sci. 138 (24) (2021) 50578.
[46] X. Zhong, et al., Maleic anhydride-β-cyclodextrin functionalized magnetic nanoparticles for the removal of uranium (VI) from wastewater, Crystals 12 (12) (2022) 1731.
[47] R. Jahanban-Esfahlan, et al., Multi-stimuli-responsive magnetic hydrogel based on Tragacanth gum as a de novo nanosystem for targeted chemo/hyperthermia treatment of cancer, J. Mater. Res. 36 (2021) 858–869.
[48] H. Ren, et al., β-Cyclodextrin-functionalized copolymers based on multiple intermolecular forces for enhanced oil recovery, Polym. Eng. Sci. 60 (10) (2020) 2581–2592.
[49] N. Tarannum, D. Kumar, Synthesis and characterization of copolymers of β-cyclodextrin derivatives, J. Indian Chem. Soc. 100 (5) (2023) 100976.
[50] T. Frison, et al., Insights on chemical reactions and formation process of electron beam-cured acrylic networks, Macromolecules 57 (3) (2024) 1291–1301.
[51] M. Dolati, et al., Multi-stimuli-responsive starch/MnO2 microparticles hydrogel for synergistic chemoradiotherapy of breast cancer, Int. J. Polym. Mater. Polymeric Biomater. 73 (9) (2024) 723–735.
[52] S. Zare, et al., Thermal-and radiation-sensitive hydrogel based on hydroxyethyl cellulose and manganese dioxide nanoparticles for synergistic chemoradiotherapy of breast cancer, Carbohydr. Polym. Technol. Appl. 6 (2023) 100394.
[53] A. Khani, et al., A novel stimuli-responsive magnetic hydrogel based on nature-inspired tragacanth gum for chemo/hyperthermia treatment of cancerous cells, J. Polym. Res. 29 (4) (2022) 149.
[54] S. Vandghanooni, et al., AS1411 aptamer-decorated cisplatin-loaded poly(lactic-co-glycolic acid) nanoparticles for targeted therapy of miR-21-inhibited ovarian cancer cells, Nanomedicine 13 (21) (2018).
[55] K. Soleimani, et al., A novel bioreducible and pH-responsive magnetic nanohydrogel based on β-cyclodextrin for chemo/hyperthermia therapy of cancer, Carbohydr. Polym. 252 (2021) 117229.
[56] T. Girek, D.-H. Shin, S.-T. Lim, Polymerization of β-cyclodextrin with maleic anhydride and structural characterization of the polymers, Carbohydr. Polym. 42 (1) (2000) 59–63.
[57] C. Henriquez, et al., Thiols as chain transfer agents in free radical polymerization in aqueous solution, Polymer 44 (19) (2003) 5559–5561.
[58] A.B. Lowe, Thiol-ene "click" reactions and recent applications in polymer and materials synthesis: a first update, Polym. Chem. 5 (17) (2014) 4820–4870.

[59] B. Massoumi, et al., A novel multi-stimuli-responsive theranostic nanomedicine based on Fe3O4@Au nanoparticles against cancer, Drug Dev. Ind. Pharm. 46 (11) (2020) 1832–1843.
[60] A.M. Musuc, et al., Development and characterization of orally disintegrating tablets containing a captopril-cyclodextrin complex, Pharmaceutics 12 (8) (2020) 1–18.
[61] Y. Fu, W.J. Kao, Drug release kinetics and transport mechanisms of non-degradable and degradable polymeric delivery systems, Expet Opin. Drug Deliv. 7 (4) (2010) 429–444.